INL/CON-14-31248
PREPRINT

EFFECTS OF THE FOIL FLATNESS ON THE STRESS-STRAIN CHARACTERISTICS OF U10MO ALLOY BASED MONOLITHIC MINI-PLATES

Proceedings of the ASME 2014 International Mechanical Engineering Congress & Exposition

Hakan Ozaltun, Pavel Medvedev

November 2014

The INL is a
U.S. Department of Energy
National Laboratory
operated by
Battelle Energy Alliance

Proceedings of the ASME 2014 International Mechanical Engineering Congress & Exposition
IMECE2014
November 14-20, 2014, Montreal, CANADA

IMECE2014 - 36605

EFFECTS OF THE FOIL FLATNESS ON THE STRESS-STRAIN CHARACTERISTICS OF U10MO ALLOY BASED MONOLITHIC MINI-PLATES

Hakan Ozaltun
Idaho National Laboratory
Idaho Falls/ID – USA

Pavel Medvedev
Idaho National Laboratory
Idaho Falls/ID – USA

ABSTRACT

The effects of the foil flatness on stress-strain behavior of monolithic fuel mini-plates during fabrication and irradiation were studied. Monolithic plate-type fuels are a new fuel form being developed for research and test reactors to achieve higher uranium densities. This concept facilitates the use of low-enriched uranium fuel in the reactor. These fuel elements are comprised of a high density, low enrichment, U–Mo alloy based fuel foil encapsulated in a cladding material made of Aluminum.

To evaluate the effects of the foil flatness on the stress-strain behavior of the plates during fabrication, irradiation and shutdown stages, a representative plate from RERTR-12 experiments (Plate L1P756) was considered. Both fabrication and irradiation processes of the plate were simulated by using actual irradiation parameters. The simulations were repeated for various foil curvatures to observe the effects of the foil flatness on the peak stress and strain magnitudes of the fuel elements.

Results of fabrication simulations revealed that the flatness of the foil does not have a considerable impact on the post fabrication stress-strain fields. Furthermore, the irradiation simulations indicated that any post-fabrication stresses in the foil would be relieved relatively fast in the reactor. While, the perfectly flat foil provided the slightly better mechanical performance, overall difference between the flat-foil case and curved-foil case was not significant. Even though the peak stresses are less affected, the foil curvature has several implications on the strain magnitudes in the cladding. It was observed that with an increasing foil curvature, there is a slight increase in the cladding strains.

Keywords: *U10Mo, Monolithic Fuel Plate, Irradiation, Foil Flatness, Finite Element Analysis*

1. INTRODUCTION

Part of Global Threat Reduction Initiative (GTRI) program, High Performance Research Reactors Fuel Development (HPRR-FD[(1)]) program has operated with the primary objective of developing the essential technologies to minimize the use of highly enriched uranium (HEU) in civilian applications. The principle vehicle by which this goal is sought is through the conversion of research and test reactors to the use of low-enriched uranium fuels (LEU, <20% ^{235}U) [1]. However, lower uranium enrichment requires higher fuel densities either as dispersion fuels at high volume loading, or in a monolithic form to compensate lower fission rates.

For the conversion of high performance research reactors to low enrichment Uranium fuel, U-Mo alloy based fuels in monolithic form were proposed. These plate-type fuels consist of a high uranium density, LEU foil contained within a diffusion barrier, and encapsulated within a cladding. Materials for these fuel elements are U-10Mo for the fuel foil, Zirconium for the diffusion barrier and Al6061-O for the cladding. For the foil material, various alloys were evaluated and it was found that U-Mo alloys are the most promising candidate for this purpose. Molybdenum extends the stability of the cubic gamma phase and this phase is known to be stable under typical irradiation conditions. Additionally, U-Mo alloy has a low neutron capture cross-section, good irradiation behavior, and an acceptable swelling response [2-4].

Early RERTR experiments indicated that the presence of an interaction layer between the fuel and the cladding materials causing mechanical problems. To minimize the potential fuel-cladding interaction, several design modifications were proposed. One of them is an inclusion of a diffusion barrier between the fuel and the cladding materials. The plates with diffusion barriers with 0.025 mm thick Zirconium produced a satisfactory irradiation performance.

✉ Corresponding Author: Email address: Hakan.Ozaltun@inl.gov
Tel: (208) 526 0274 | Fax: (208) 526 2930

(1) Formerly RERTR, Reduced Enrichment for Research and Test Reactors

Several steps involve in the fabrication process of a monolithic plate. The initial stage of the fabrication process is the preparation of coupons made of U10Mo alloy. For this, Uranium and Molybdenum feedstock is melted in an inert atmosphere and casted into thin sheets. Then, the sheets are machined or rolled to produce thin coupons. In order to control inter-diffusion phenomenon which occurs at the fuel-cladding interface during the irradiation process, U10Mo coupons are laminated with Zirconium diffusion barrier prior the hot rolling process.

To apply Zirconium liners on each faces of the coupons, co-rolling technique is used. For this, U10Mo coupon is placed between two thin Zirconium layers (Zr-U10Mo-Zr). Then, layers are positioned in a frame made of low carbon steel. Cover plates are placed to the top and bottom of the layers; and finally, the assembly is welded before the rolling process. The sheets are hot rolled at approximately 650 °C. Multiple hot rolling passes is performed to minimize occurrence of micro cracks. Typical number of hot passes is 20-40 for the preparation of a 0.25-0.50 mm thick Zr-U10Mo co-rolled foil. Once reduction via hot co-rolling is completed, the coupon assembly is placed into a furnace for 45 minutes at 650 °C to reduce the residual stresses and minimize the material anisotropy. Finally, heat treated Zr-U10Mo co-rolled foils are removed from the rolling assembly by trimming the perimeters of coupons.

The final stage of the foil preparation is to reduce the thickness of Zr-U10Mo co-rolled foil to its targeted value via cold rolling process. Typical thickness reduction is 0.015-0.025 mm per pass. Final thickness of the co-rolled foil varies depending on the reactor application. The cold rolling process creates smoother foil surfaces and lead to more uniform foil thickness facilitating higher quality of the bonds during subsequent Hot Pressing process [5-7].

Finally, the co-rolled foils are encapsulated in a cladding material via Hot Isostatic Pressing (HIP), completing the fabrication process. For this, a co-rolled foil (trimmed to target dimensions prior HIP) is placed between two layers of Aluminum cladding material (Al6061-O for RERTR fuel plates). These layers are subjected to a HIP procedure conducted at a temperature of 560 °C and a pressure of 104 MPa for 90 minutes before being cooled to room temperature at a rate of 4.8 °C/min with diminishing the pressure as described in details elsewhere [8]. Once the HIP process is completed, the fuel plates have a total thickness of 1.397mm. These plates are then trimmed to 101.473 mm x 25.400 mm. Inside the cladding, the foil and liners have a nominal thickness of 0.254 mm and 0.0254 mm, respectively. Nominal dimensions of the final product are shown in *Fig.1a*.

Mini-plates are then assembled into capsules made of AL6061-T6. There are 4 capsules named A, B, C and D from top to bottom, and each capsule can hold 8 mini-plates. Containing 32 mini-plates, the capsule assembly is then positioned vertically in a basket. The plates are cooled by a direct contact with the primary coolant.

There are concerns that if the flatness of the foil has implications on stress-strain behavior of the plates and on overall irradiation performance, as it is not always the case to fabricate the plates with perfectly flat fuels in the center. The aim of this work is to investigate and characterize these effects. Over the course of this study, the fully coupled thermo-mechanical behavior of a selected plate was simulated. Between the simulations, curvature of the foil was varied from perfectly flat case to the limiting case. A comparative evaluation was made to determine the sensitivity of the plate's performance to the flatness of the fuel foil.

In this study, the plate L1P756 from RERTR-12 test matrix was considered. This plate was irradiated at frontal neutron flux configuration (face-on orientation) in position D-5 (the bottom row of Capsule D). The plate was in 1st slot in the capsule, between the coolant channels 1 and 2. This setup was shown schematically in *Fig.1b.*

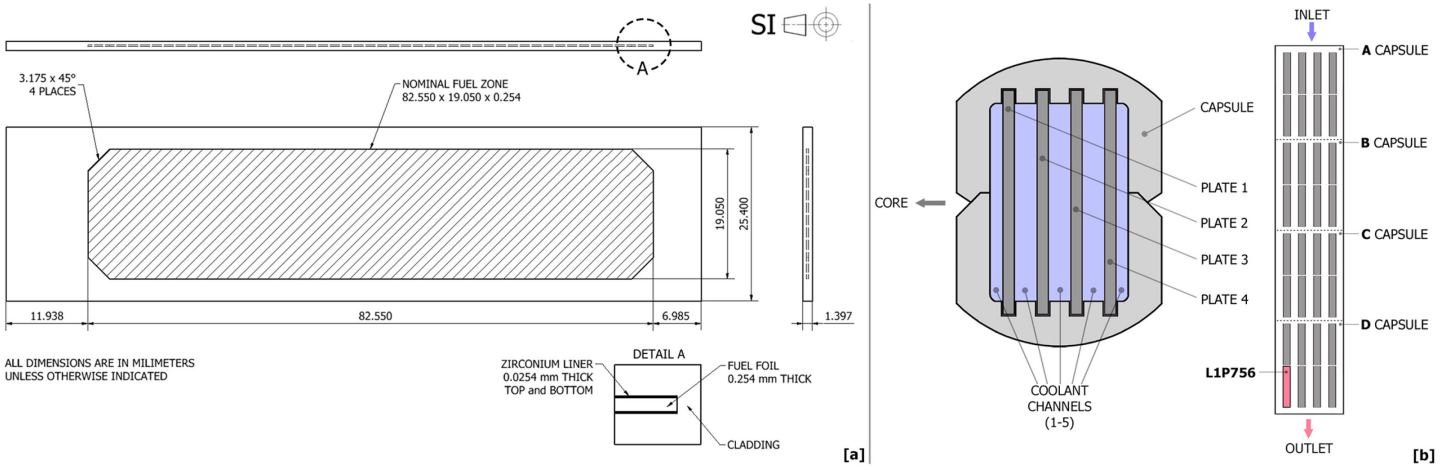

Figure 1 (a) Mini-plate dimensions that were used in the model **(b)** Capsule, coolant channels and position of L1P756

2. IRRADIATION PARAMETERS

The plate L1P756 was irradiated in 2 cycles of RERTR-12. Total irradiation time for the plate was 89.7 days. Effective irradiation times with respect to cycles are 50.5 days in cycle 146A; and, 39.2 days in cycle 146B.

The experimental data for the fission power density, fast neutron flux, fast neutron fluence and average fission density for these 2 cycles are summarized in *Table 1*. These variables were implemented via utility subroutines accordingly. In the models, a linear interpolation was used to estimate the values between the known data points. In *Fig.2*, resulting models and their comparison with experimental data are shown.

Due to a frontal flux orientation, local to average ratio (L2AR) of the fission density varies with respect to spatial coordinates. *Fig.3* shows the fission density L2AR in axial direction (*Fig.3a*), in transverse direction (*Fig.3b*), and actual 2D mapping with respect to spatial coordinates (*Fig.3c*).

It is important to note that an accurate implementation of the fission density is crucial for the fidelity of the results, as many irradiation parameters are affected by the local fission density;

Table 1 Irradiation Parameters for the plate L1P756 [9]

Irradiation Cycle	Irradiation Time		Fission Power Density	Fast Neutron Flux	Fast Neutron Fluence	Average Fission Density
	[days]	[hours]	[W/cm^3]	[n/m^2-sec]	[n/m^2]	[fission/m^3]
146A 50.5 EFPD	0	0	31410.95	2.06E+18	0.00E+00	0.00E+00
	16	384	29244.27	2.08E+18	2.85E+24	1.45E+27
	32	768	28252.78	2.03E+18	5.73E+24	2.80E+27
	50.5	1212	27111.33	1.99E+18	8.98E+24	4.31E+27
146B 39.2 EFPD	50.5	1212	24908.87	1.71E+18	8.98E+24	4.31E+27
	68.5	1644	23412.37	1.79E+18	1.16E+25	5.60E+27
	78.5	1884	22923.41	1.77E+18	1.32E+25	6.28E+27
	89.7	2152.8	22334.53	1.75E+18	1.49E+25	7.03E+27

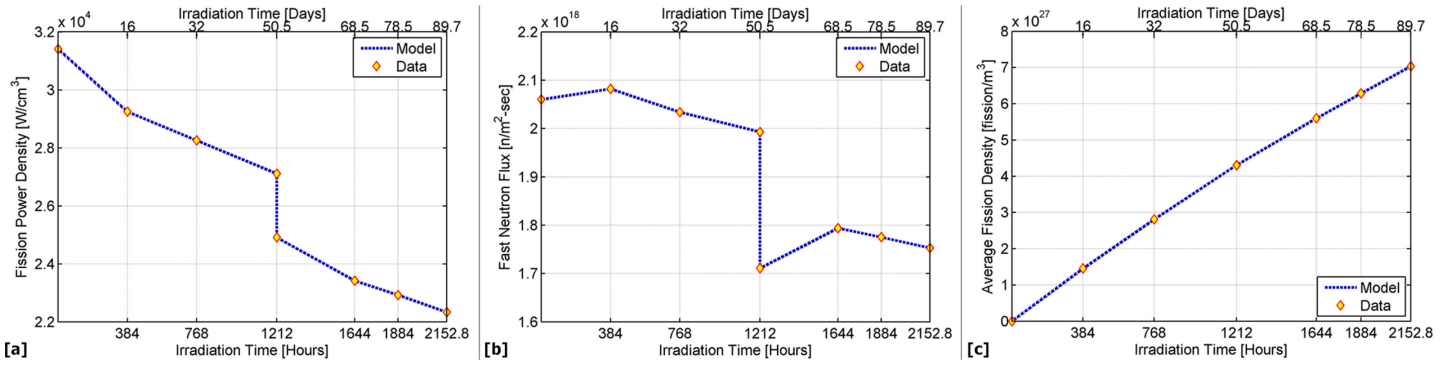

Figure 2 Irradiation Parameters **(a)** Fission Power Density **(b)** Fast Neutron Flux **(c)** Average Fission Density

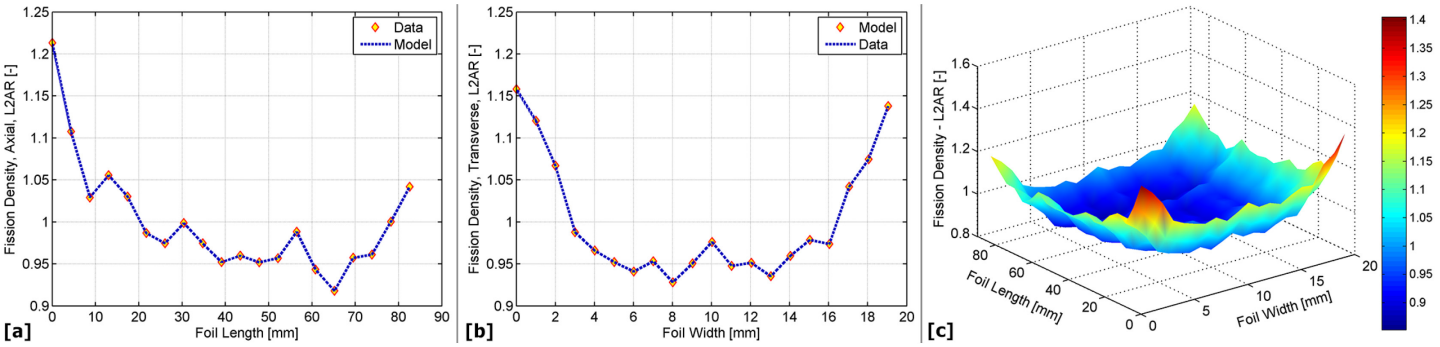

Figure 3 Fission Density, L2AR **(a)** Axial direction **(b)** Transverse direction **(c)** 2D field over the foil

such as, volumetric heat generation, foil swelling, irradiation creep, conductivity degradation etc.

The average fission density in the fuel foil was constructed as a linear interpolation of ordered pairs of average fission density and time shown in *Fig.2c*. This function is called on each material point to return the value of the average fission density. The value for the local to average fission density ratio along the lengthwise and widthwise edges of the foil was implemented at twenty points, which are spaced equally from each other along those respective spatial dimensions. Linear interpolations were used to calculate L2AR between the grid points in the length and width directions. The resulting interpolation values were multiplied (bi-linear interpolation) to yield a surface mapping field of the L2AR fission density across the fuel foil as shown in *Fig.3c*. Finally, the local fission density at a given time was calculated as the product of the average fission density and the local to average fission density ratio at each material point within the fuel foil.

Volumetric heat generation rate due to fissions is shown in *Fig.2a.* Data for the average power density was gathered from the neutronics calculations and it was implemented as a function of the irradiation time. Between the time points, a linear interpolation was used to approximate the fission power density at a specific irradiation time. The average fission power density (*Fig.2a*) was then multiplied by the Local to Average Ratio of the fission density (*Fig.3c*) to calculate the local volumetric heat generation at a specific location and time. This procedure was repeated for the each material point.

Shown in *Fig.2b*, the data for the fast neutron flux was gathered from the neutronics calculations. Similar with the heat generation rate, it was also implemented as a function of irradiation time. A linear interpolation was used to calculate the flux and fluence at a specific time for each material point. Values for the fast neutron fluence were used to simulate the irradiation effects on Al6061 cladding and Zirconium liner. These irradiation effects that were considered in this work are irradiation hardening, swelling and creep.

3. FINITE ELEMENT MODEL

The geometric model was created by using the nominal dimensions that were shown in *Fig.1*. A full model was utilized to account the different temperature profiles for different channels and the coolant temperature increase in the channels.

C3D8RT element of ABAQUS, an 8-node thermally coupled brick, tri-linear displacement and temperature with reduced integration and hourglass control, was used. Chamfered edges were represented by 7x7x10 nodal divisions. Equally spaced 4 layers were used to represent the thickness of the foil. Nodal divisions along the length and width directions are 174 and 42, respectively. A total number element on the foil was 29168 bricks. Equally spaced 3 layers were used to represent the thickness of the Zirconium liner. Similar with the foil, each of the Zirconium liners utilized 174 and 42 divisions along its length and width direction, respectively. This resulted 21876 hexahedral for one liner, and total 43752 hexahedral for the both liners. The thickness of the cladding material was represented by 16 layers. The nodal divisions along the length and the width directions of the cladding are 214 and 56, respectively. The total number element on the cladding was 121448.

For all four parts of the plate, a mapped meshing with sweeping technique was used to match the elements and the nodal points at the interfaces. The total number of elements in the plate was 194368 hexahedral. Resulted finite element discretization of the geometry is shown in *Fig.4*.

It was assumed that the bonding between the foil, cladding and Zr liner are ideal and there are no defects present prior irradiation. It was also assumed that no interfacial delamination occurs during the irradiation process. Therefore, all nodal points at the interfaces were tied together. The plate was modeled as free to move in all directions, except along its long edges. At the longitudinal edges, only the sliding motion was permitted, as these edges are constrained by the rails of the capsule. One single node on cladding corner was fixed to prevent rigid body motion.

For this work, two consecutive simulations were performed, namely, fabrication and irradiation. Irradiation simulation used the stress-strain results from the fabrication simulation as an initial state for the irradiation. Residual stress and strain fields caused by the cooling stage of the HIP process were calculated via a fully coupled, temperature-displacement simulation.

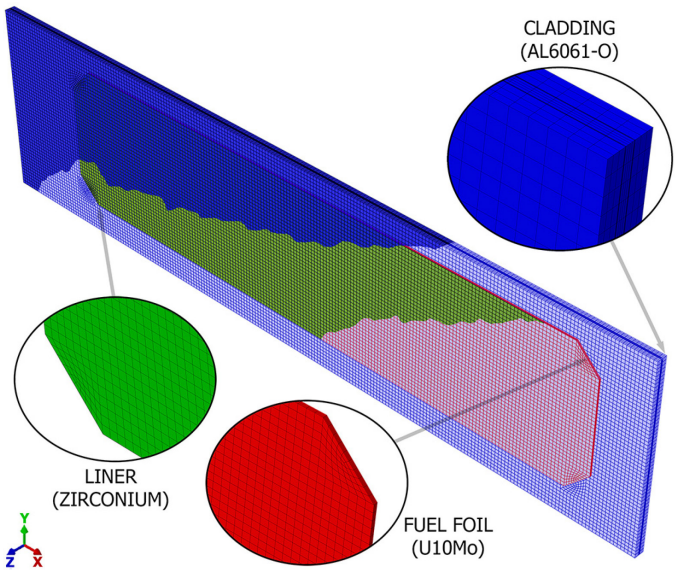

Figure 4 3D Model and FE discretization

Fabrication simulation was built by using a transient step of 6737 seconds with a predefined initial and a final temperature fields. The predefined temperature field was 560 °C (HIP temperature) and was uniform throughout the plate. The subsequent step introduced a room temperature as a boundary condition across the surface of the plate, and the temperature was then allowed to decrease during the transient. Cooling rate was 4.8 °C/min. Symmetry condition was applied to the corresponding nodes at the mid-plane of the plate. A single node at the volumetric center was fixed to prevent rigid body motion. The results of this simulation were then passed to the irradiation simulation to define the initial state.

Irradiation process was modeled for 2152.8 hours (89.7 days). Time history was divided into 2 sub-steps for each irradiation cycles (cycle 146A and cycle 146B). Irradiation cycle 146A was simulated for 1212 hours (50.5 days) followed by 146B for 940.8 hours (39.2 days).

To implement the field variables, ABAQUS utility subroutines were created accordingly. The USDFLD user routine was used to define the local fission density within the fuel foil with respect to the spatial coordinates and the irradiation time. This subroutine was also used to calculate the fast neutron flux and fluence for the cladding and the liner materials. Thermal conductivity degradation of the fuel foil was implemented as a function of the local fission density. It was introduced to the model via an independent field variable.

The irradiation induced creep and the models for the gaseous, solid and total swelling for the fuel foil was implemented in the user subroutine CREEP. Irradiation effects in the cladding material such as swelling strain and neutron hardening was included in this routine also.

The fission power density of the fuel foil was introduced as a body heat flux in the model. Local volumetric heat generation of the foil was calculated by using L2AR of the fission density. Heat transfer calculations between the plate surface and the primary coolant were performed by using Petukhov correlation. A film condition was created on the cladding surface and experimental coolant channel temperatures were used for the channel definition.

Plate edges along the lengthwise and widthwise directions were constrained (sliding only) to simulate the mechanical restrictions resulted by the fuel capsule restraints. A single node at the outer corner of the plate was fixed to prevent rigid body motion.

A fully coupled thermal-displacement transient solver with active swelling-creep-viscoelastic behavior was used. An explicit-implicit integration scheme was selected for the solver. Maximum time increment per step was set to be 12 hours and maximum temperature increment per step was set to be 5 °C to avoid numerical instabilities.

4. MATERIAL MODELS

Material models that were used in this study are: U10Mo for the fuel, Zirconium for the liner, AL6061-O for the cladding, and light water at 2.52 MPa for the coolant models. Material properties that were used for the model are in *Appendix A*.

Model for the thermal conductivity degradation of the fuel material was adapted from Hayes [10] and expressed by,

$$k_p = k_0 \times e^{(-2.14 \times P)} \tag{1}$$

where k_0 is the thermal conductivity of the fully dense material, P is the porosity factor (valid for $P \leq 0.3$) and k_p is the thermal conductivity of the porous medium.

Porosity factor, P was calculated via,

$$P = \frac{(\Delta V/V_0)_g}{(\Delta V/V_0)_g + 1} \tag{2}$$

where $(\Delta V/V_0)_g$ is swelling due to the gaseous products. The model for the gaseous swelling was adapted from [11] as,

$$\left(\frac{\Delta V}{V_0}\right)_g = 1.0 \cdot f_d \qquad f_d \leq 3\times10^{27} \text{ fis/m}^3 \tag{3}$$

$$\left(\frac{\Delta V}{V_0}\right)_g = 3.0 + 2.3\cdot(f_d - 3) + 0.33\cdot(f_d - 3)^2 \qquad f_d > 3\times10^{27} \text{ fis/m}^3 \tag{4}$$

where $(\Delta V/V_0)_g$ gaseous swelling in (%) and f_d is local fission density in $\times10^{27}$ (fissions/m^3).

Irradiation induced creep model is based on Kim [12] as,

$$\dot{\varepsilon} = A \cdot \sigma \cdot \dot{f} \tag{5}$$

where, $\dot{\varepsilon}$ is creep strain rate (1/sec), A is irradiation creep coefficient (500×10^{-25} cm^3/MPa-fis), σ is equivalent stress (MPa) and $\dot{f}$ is fission density rate (fissions/cm^3-sec).

The model for the fuel meat swelling due to fission products is based on the relation given by Kim [11] as,

$$\left(\frac{\Delta V}{V_0}\right)_f = 5.0 \cdot f_d \qquad f_d \leq 3\times10^{27} \text{ fis/m}^3 \tag{6}$$

$$\left(\frac{\Delta V}{V_0}\right)_f = 15 + 6.3\cdot(f_d - 3) + 0.33\cdot(f_d - 3)^2 \qquad f_d > 3\times10^{27} \text{ fis/m}^3 \tag{7}$$

where $(\Delta V/V_0)_f$ total volumetric swelling of the fuel in (%), and f_d is the local fission density in $\times10^{27}$ (fissions/m^3).

5. COOLANT CHANNEL MODEL

Models for thermo-physical properties of the water were develop via the data reported by NIST [13]. Mathematical relations were developed for the coolant at 2.52 MPa, the nominal operating pressure of ATR. Valid temperature range for the models is 1-100 °C. In the models, T is in °C.

Density (kg/m^3) was defined according to

$$\rho = 1.46\times10^{-5}\cdot T^3 - 5.664\times10^{-3}\cdot T^2 + 3.318\times10^{-3}\cdot T + 1001 \quad (8)$$

The model for the specific heat (J/kg-K) is

$$C_p = 2.462\times10^{-6}\cdot T^4 - 6.120\times10^{-4}\cdot T^3 + 6.169\times10^{-2}\cdot T^2 - 2.459\cdot T + 4206 \quad (9)$$

Thermal diffusivity model (m^2/sec) is

$$\alpha = -2.068\times10^{-12}\cdot T^2 + 5.562\times10^{-10}\cdot T + 1.334\times10^{-7} \quad (10)$$

The model for thermal conductivity (W/m-K) is

$$k = -9.565\times10^{-6}\cdot T^2 + 2.147\times10^{-3}\cdot T + 0.5609 \quad (11)$$

Kinematic viscosity (m^2/sec) is

$$\nu = 3.009\times10^{-14}\cdot T^4 - 8.433\times10^{-12}\cdot T^3 + 9.291\times10^{-10}\cdot T^2 - 5.321\times10^{-8}\cdot T + 1.758\times10^{-6} \quad (12)$$

Dynamic viscosity (Pa-s) is

$$\mu = 2.986\times10^{-11}\cdot T^4 - 8.382\times10^{-9}\cdot T^3 + 9.259\times10^{-7}\cdot T^2 - 5.332\times10^{-5}\cdot T + 0.00176 \quad (13)$$

The model for Prandtl Number is

$$Pr = 2.632\times10^{-7}\cdot T^4 - 7.336\times10^{-5}\cdot T^3 + 7.970\times10^{-3}\cdot T^2 - 0.4396\cdot T + 13.13 \quad (14)$$

Reynolds Number was calculated according to

$$Re = \frac{\rho\cdot v\cdot D_H}{\mu} \quad (15)$$

Where, v is velocity and D_H is hydraulic diameter. Coolant velocities are, 12.61 m/sec and 10.18 m/sec for inner and outer channels, respectively. Hydraulic diameter (D_H) is

$$D_H = 4A/P \quad (16)$$

where A is the cross sectional area and P is the wetted perimeter of the cross-section.

For L1P756 plate in position D5, the channel widths are 1.4986 mm for the outer channel (Channel 1). The inner channel (Channel 2) is 2.3876 mm wide (1.1938 was used due to a channel symmetry). The channel length is 22.555 mm for the both channels.

Nusselt number was calculated by using Petukhov-Gnielinski correlation [14]. For a fully developed turbulent and transition flow (Re > 2300), the Nusselt number is given by

$$Nu = \frac{\left(\frac{f}{8}\right)\cdot(\mathrm{Re}-1000)\cdot\mathrm{Pr}}{1+12.7\cdot\left(\frac{f}{8}\right)^{1/2}\cdot\left(\mathrm{Pr}^{2/3}-1\right)} \quad (17)$$

Where, Pr is the Prandtl number ($0.5 \le \mathrm{Pr} \le 2000$), Re is the Reynolds number ($3000 < \mathrm{Re} < 5\times10^6$) and f is the friction factor from the first Petukhov equation.

Friction factor in *Eqn.17* was calculated according to

$$f = \left(\frac{1}{0.790\cdot\ln(Re)-1.64}\right)^2 \quad (18)$$

The heat transfer coefficient was calculated by

$$h = \frac{k}{D_H}\cdot Nu \quad (19)$$

where, h is heat transfer coefficient (W/m^2-K), k is thermal conductivity (W/m-K), D_H is hydraulic diameter (m), Nu is the Nusselt Number.

The heat transfer between the coolant and the plate surface was simulated by creating a surface interaction, which defines a film condition at the plate surfaces. Surface film condition was created by using coolant temperatures reported in [9] and calculated heat transfer coefficients (*Eqn.17*) shown in *Fig.5*.

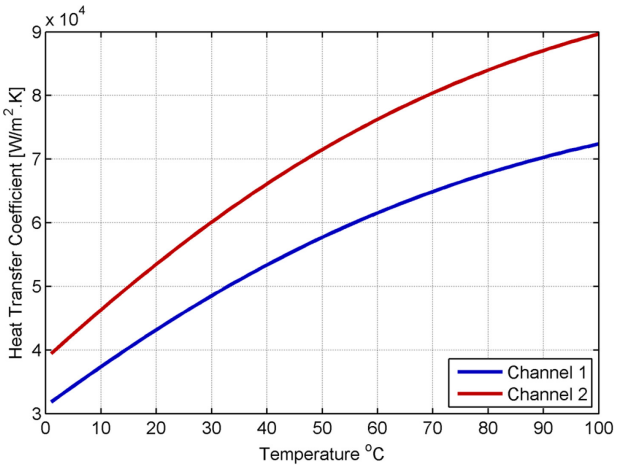

Figure 5 Heat transfer coefficient for the channels

6. RESULTS AND DISCUSSIONS

6.1. Fabrication (HIP)

The fabrication model simulated the cooling stage of the HIP process from 560 °C to 21°C. Cooling time to reach a steady state is 6737 seconds. The cooling rate is 4.8 °C/min. *Fig.6* shows the stress-strain fields at the end of the cooling stage.

Shown in *Fig.6a*, the equivalent stress contour indicates that the foil stresses would be ranging from 140 MPa to 296 MPa. Peak stresses are located at the foil ends. Lowest stresses are located on the perimeter of the foil.

The stress field in the Zr-liner is shown in *Fig.6b*. Even though stresses in the liner have similar patterns with those in the foil, the magnitudes in the liner are higher. Stresses are ranging from 329 to 344 MPa.

Fig.6c shows the equivalent stresses in the cladding. The peak stresses (70.13 MPa) are found to be at the interface region with Zr-liner and at the contact area with the perimeter of the foil. Equivalent strain field in cladding is in *Fig.6d*. The peak strains are computed to be 0.601%. In figure, the detailed view from the *x-y plane* (mid-plane) reveals that the peak cladding strains are at the perimeter of the contact region with the fuel foil.

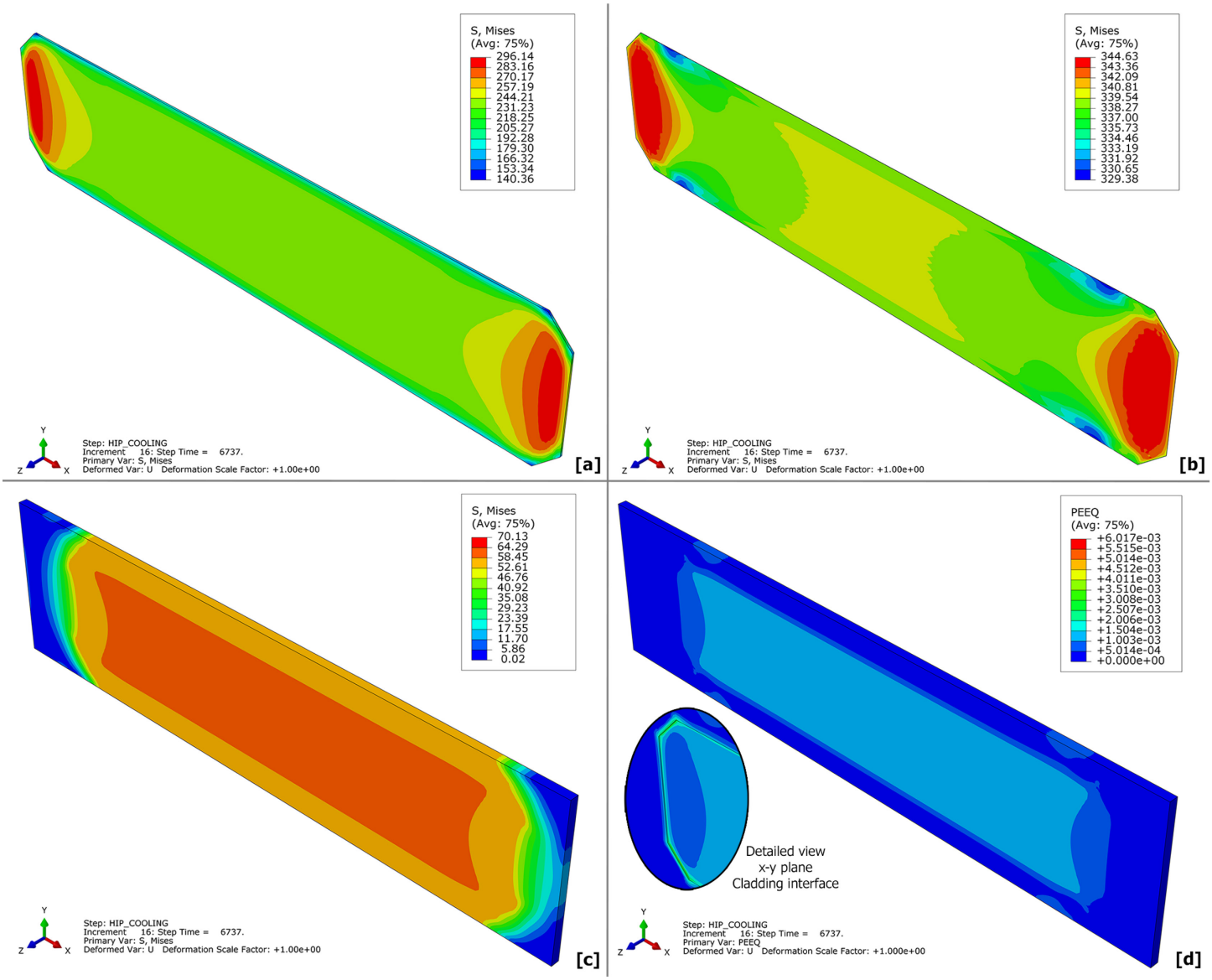

Figure 6 End of fabrication process, Contours are showing
(a) Equivalent stress [MPa] in the fuel foil **(b)** Equivalent stress [MPa] in Zr liner
(c) Equivalent stress [MPa] in the cladding **(d)** Equivalent plastic strains [mm/mm] in the cladding

6.2. Irradiation

To evaluate the plate performance, irradiation of the plate L1P756 was simulated for 2152.8 hours (89.7 days) via 2 sub-steps, namely, cycle 146A for 50.5 EFPD and cycle 146B for 39.2 EFPD. The temperature fields for the end of the cycle 146B (end of irradiation) are shown in *Fig.7*.

In the figure**,** the temperature fields of the foil at the interface with the Zirconium liner (*Fig.7a*); and, at the foil centerline (*Fig.7b*) are shown. Results are for the end of the irradiation, at which, the plates are at 22334.53 [W/cm^3] power, just before the reactor shutdown.

The peak foil temperatures were found to be in the inlet side, where the fission densities are the highest. Calculated peak foil temperatures are 130.98 °C (404.13 °K) at the interface (*Fig.7a*) and 179.61 °C (452.76 °K) at the centerline (*Fig.7b*). Minimum foil temperature was calculated to be 86.01 °C (359.16 °K) around the foil perimeter.

The temperature fields for the cladding at the interface and at the plate surface are shown in *Fig.7c* and *Fig.7d* From the figures, the peak temperatures for the cladding are 126.40 °C (399.55 °K) at the interface, and 109.23 °C (382.38 °K) at the surface. The lowest cladding temperature is 68.26 °C (341.41 °K). The peaks are closer to the inlet side.

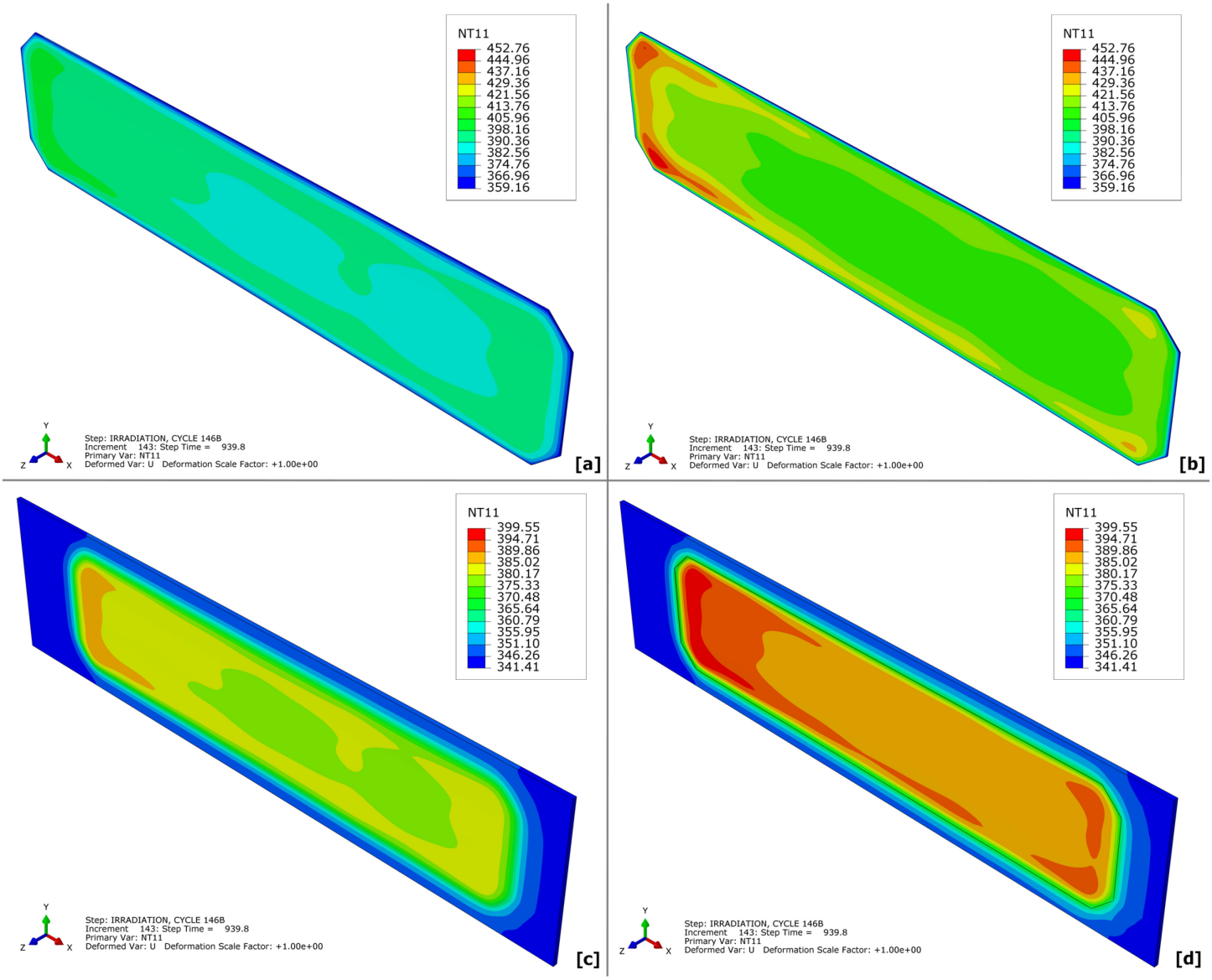

Figure 7 Temperature [°K] fields, End of irradiation, (end of cycle 146B, 89.7 days, at 22334.53 [W/cm^3]), contours are showing
(a) Foil temperature [°K] at the interface **(b)** Foil temperature [°K] at the center line
(c) Cladding temperature [°K] at the surface **(d)** Cladding temperature [°K] at the interface

The fission density on the foil reaches to 9.15×10^{27} [fis/m^3] with L2AR of 1.302 at the inlet side as seen in *Fig.8a*. The calculated swelling strain due to gaseous products on the foil is in *Fig.8b*. From the figure, the minimum gaseous swelling on the foil is 13.02%. Reaching to its peak closer to the inlet side, the maximum gaseous swelling is 29.64%.

The large gaseous swelling has implications on the integrity of the foil. It is shown that the gaseous swelling has a critical breakaway value and can be used to predict a failure [15]. It was formulated that when the gaseous swelling approaches 33.3%, the bubbles touch neighboring bubbles in a randomly arranged configuration, assisting interconnection of the pores, and thus, facilitating escape of the gaseous products to the surface. It is also reported that an upper limit of 30% for gaseous swelling is often observed [15-17]. By using this information, it may be claimed that if the gaseous swelling increases beyond 30% foil may become critical and any gaseous swelling above 33.3% may lead to a breakaway failure. A closer examination of swelling results in *Fig.8b* indicates that no regions in the fuel foil reach to a critical breakaway value that would cause a breakaway failure.

In *Fig.8c*, contour mapping for the irradiation induced creep in the fuel is shown. The minimum creep strain is 21.9 % at the mid-section of the foil. The larger creep strain is observed around the entire perimeter of the foil. The peak irradiation creep strain is 79.1% and it is located at the inlet side.

Shown in *Fig.8d*, the displacement contours in the thickness direction reveals a bulging. The maximum displacement in the thickness direction was computed to be 0.240 mm (0.120 mm

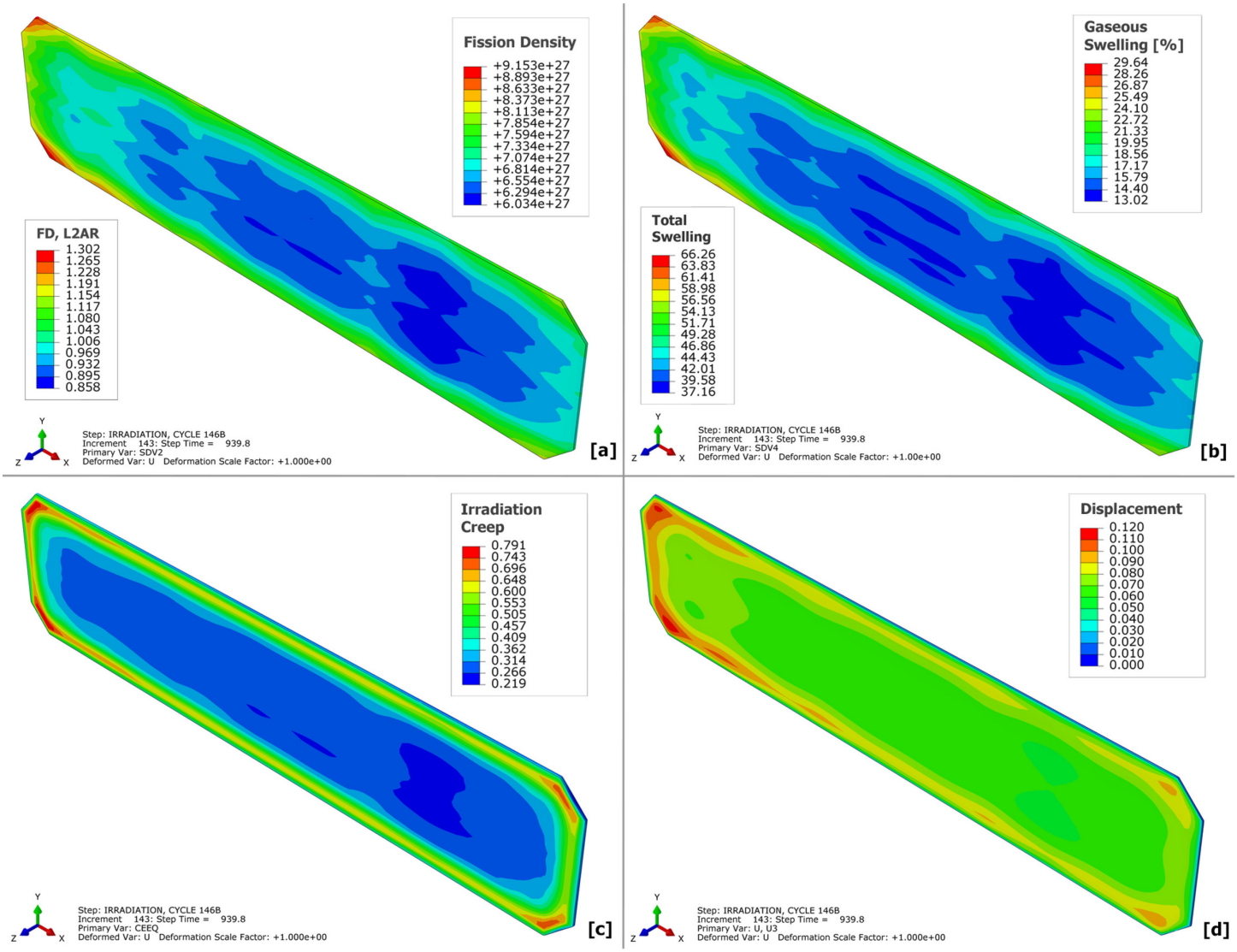

Figure 8 Contour plots for the foil at the end of the irradiation process
(a) Local fission density [fis/m^3] and L2AR **(b)** Gaseous swelling [%] and regions with 33.3% and more gaseous swelling
(c) Irradiation induced creep strain in the foil **(d)** Total displacement [mm] of the foil in the thickness direction

with respect to the mid-plane) at the inlet side. This corresponds to approximately 95% swelling. Other regions of high displacements are observed at the perimeter of the foil.

Equivalent stress fields for the foil, cladding and liner materials are shown in *Fig.9*. The stress fields at the end of the irradiation (end of the cycle 146B, plate at 22334.52 W/cm^3 power) can be seen in *Fig.9a*. The results indicate that the stresses on the foil are negligible. However, the residual stresses would develop during the shutdown as shown in *Fig.9b*. From the figure, an equivalent stress of 70 MPa is present on the regions closer to the inlet side.

Prior irradiation, residual stresses due to the fabrication process on the foil were ranging from 140 MPa to 296 MPa as discussed in *Sec.6.1*. Irradiation simulations have revealed that fabrication induced stresses in the foil are relieved in less than 12 hours due to a high irradiation creep strain. This implies that the fuel foil would be essentially stress-free in the reactor.

During irradiation, a slight decrease in the fabrication stresses in the Zr-liner is observed. Peak equivalent stress is approximately 300 MPa around the perimeter as shown in *Fig.9c*. This reduction is due to the relaxation of the foil by irradiation creep and thermal creep in Zr-liner material. Unlike the foil material, stresses in the cladding increase during irradiation. For the cladding material, the residual stress due to fabrication was computed to be 71.35 MPa. *Fig.9d* reveals that the stresses increase to 150 MPa. This is due to irradiation hardening. Additional stresses in the cladding are also produced by the strains as a result of the volumetric swelling of the foil.

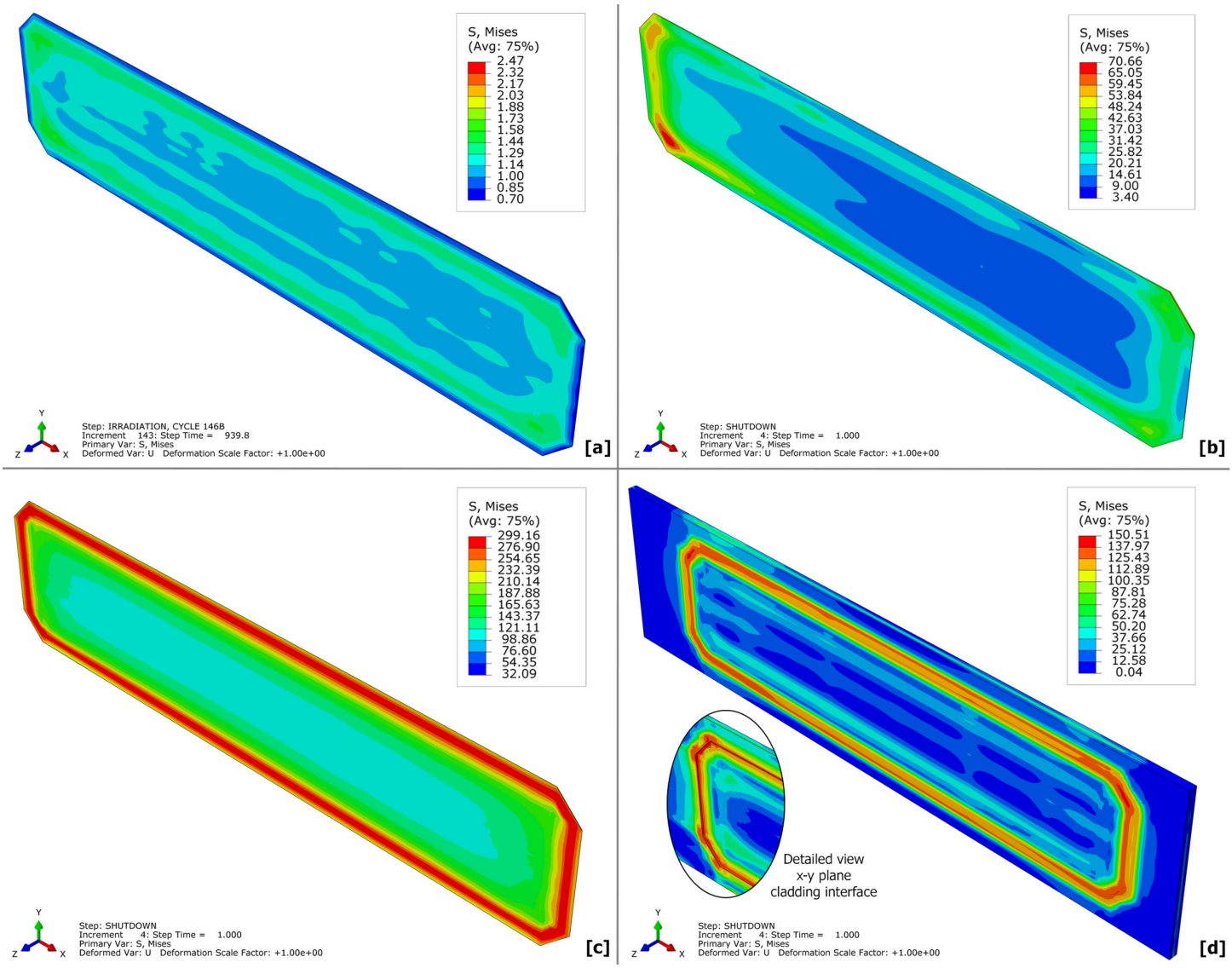

Figure 9 Equivalent stress [MPa] fields for the foil and the cladding, contours are showing **(a)** Foil, end of irradiation, (89.7 days, at 22334.53 [W/cm^3]) **(b)** Foil, centerline view, end of shutdown **(c)** Zr-liner, showing interface with the fuel, end of shutdown **(d)** Cladding, end of shutdown

6.3. Case Studies: Effects of Foil Flatness

The results for the fabrication and irradiation processes of the plate L1P756 with a centered flat foil were previously discussed. There are concerns that if the flatness of the foil has implications on stress-strain behavior of the plates and on overall irradiation performance. The aim of this section is to investigate and characterize these effects. For this, a sensitivity study was performed. Between the simulations, curvature of the foil was varied from the perfectly flat case to the limiting case as shown schematically in *Figure 10*. The limiting case is the minimum allowable cladding thickness, which is 0.152 mm.

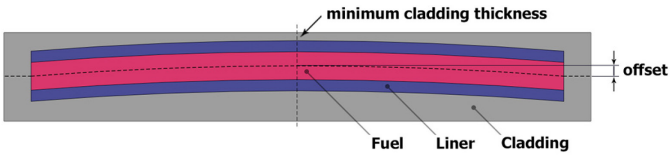

Figure 10 Foil curvature study

The new models utilized the same irradiation parameters with the previous plate (L1P756). All geometric specifics that were presented in *Fig.1* were kept unchanged, except the flatness of the foil. For the fabrication and irradiation models, total 6 distinct curvatures were evaluated as tabulated in *Table 2*.

Table 2 Evaluated cases for the plate L1P756

Cases	Foil curvature Centerline offset		Cladding thickness	Details
	[%]	[mm]	[mm]	[-]
1	0	0.000	0.5461	Nominal Thickness
2	25	0.063	0.4826	-
3	50	0.127	0.4191	-
4	75	0.190	0.3556	-
5	100	0.254	0.2921	-
6	155	0.393	0.1524	Minimum Cladding

Fig.11 shows the evolution of the peak stress-strains during fabrication and irradiation with respect to the foil curvature. The fabrication constrain for this study is the minimum allowable cladding thickness, which is defined as 0.152 mm. In the figures, the centerline offset 0.000 mm represent the nominal case (perfectly flat foil), and centerline offset of 0.393 mm is the upper bound, which corresponds to the minimum cladding thickness of 0.152 mm. Results in the figure indicated that the peak foil and cladding stresses for fabrication and irradiation parts are not affected significantly by the flatness of the foil.

The magnitudes of the peak strains are shown in *Fig.11c*. From the figure, the peak cladding strains are affected considerably by the flatness of the foil. As expected, the lowest strain magnitudes can be achieved by the flat foil (foil centerline offset = 0.000 mm). If a flatness of the foil is not preserved, the peak cladding strains increase roughly 50%. Once it is deviated, further changes of the foil curvature do not change the peak strains further.

7. CONCLUSIONS

Irradiation performance of the plate L1P756 from RERTR-12 was evaluated. The effects of the flatness of the foil on the plate's stress-strain characteristics during the fabrication, irradiation and reactor shutdown were studied.

It is found that the flatness of the foil does not impact the peak stresses as the magnitudes are comparable for various curvature distances. The stresses are slightly lower at the mid-section for the case with a flat foil. For the strain fields, evaluation of the profiles and magnitudes for various cases indicated that shape of the foil has several implications on the strain characteristics of the cladding material.

Flat foil case has provided the lowest peak strains; and thus, more desirable from mechanical perspective. On the other hand, requesting a perfectly flat foil in a plate especially after HIP might not be easy or feasible. Changes in the peak strains of the cladding material are less significant with an increasing curvature, once the flatness is strayed. While the peak strains are located at the perimeter of the bond region with the foil, the strain magnitudes in other region of the cladding are significantly lower.

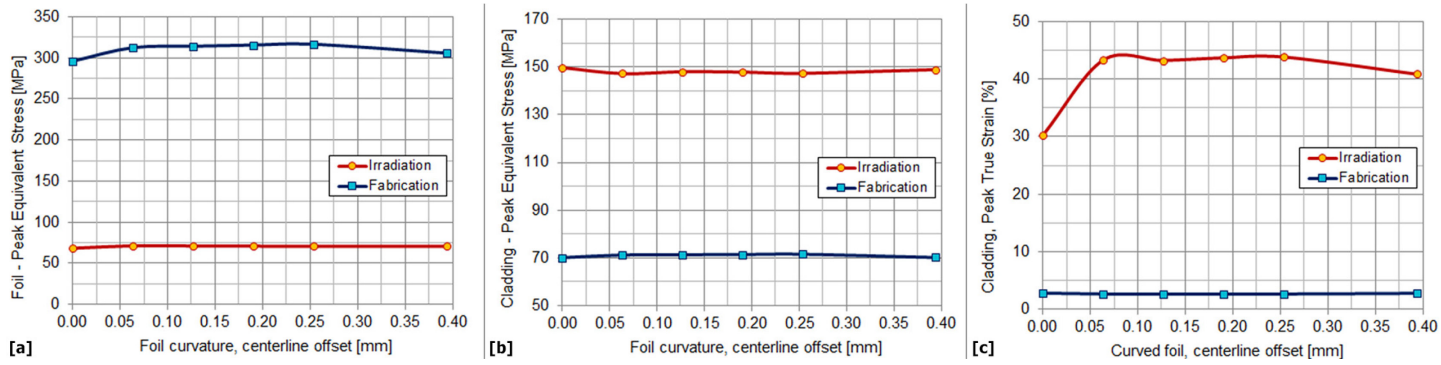

Figure 11 (a) Equivalent stresses in the fuel **(b)** Equivalent stresses in the cladding **(c)** Total strains in the cladding

NOMENCLATURE

A	Power law multiplier for irradiation creep
A_c	Cross sectional area of the coolant channel
C_p	Specific Heat
D_H	Hydraulic diameter
f	Friction factor from the first Petukhov equation
f_d	Fission density
$\dot{f}$	Fission density rate
h	Heat transfer coefficient
k	Thermal conductivity
Nu	Nusselt number
P	Porosity
P_c	Wetted perimeter of the cross-section
Pr	Prandtl number
Re	Reynolds number
V	Volume
α	Thermal diffusivity
$\dot{\varepsilon}$	Equivalent creep strain rate
μ	Dynamic viscosity
ρ	Density
$\tilde{\sigma}$	Equivalent deviatoric stress
σ_{eq}	Equivalent stress
ν	Kinematic viscosity

ACKNOWLEDGMENTS

This work was supported in part by an allocation of computing time from High Performance Computing facilities of Idaho National Laboratory.

REFERENCES

[1] J. L. Snelgrove, G. L. Hofman and M. K. Meyer, "Development of very high density low-enriched Uranium fuels," *J. Nucl. Eng. Des.,* vol. 178, p. 119–12, 1997.

[2] D. B. Lee, K. H. Kim and C. K. Kim, "Thermal compatibility studies of un-irradiated U-Mo alloys dispersed in Aluminum," *J. Nucl. Mater.,* vol. 250, pp. 79-82, 1997.

[3] M. K. Meyer, G. L. Hofman, S. L. Hayes and C. R. Clark, "Low temperature irradiation behavior of U-Mo alloy dispersion fuels," *J. Nucl. Mater.,* vol. 304, pp. 221-236, 2002.

[4] J. M. Park, K. H. Kim, C. K. Kim, M. K. Meyer, G. L. Hofman and R. V. Strain, "The irradiation behavior of atomized U-Mo alloy fuels at high temperature," *J. Met. Mater. Int.,* vol. 7, no. 2, p. 151–157, 2001.

[5] G. A. Moore and M. C. Marshall, "Co-Rolled U10Mo/Zirconium-Barrier-Layer Monolithic Fuel Foil Fabrication Process," INL/EXT 10-17774 Idaho National Laboratory Technical Report, Idaho Falls, 2010.

[6] G. A. Moore, F. J. Rice, N. E. Woolstenhulme, J. Jue and B. H. Park, "Monolithic Fuel Fabrication Process Development at the Idaho National Laboratory," in *RERTR 2009 - 31st International Meeting on Reduced Enrichment for Research and Test Reactors*, Beijing, China, 2009.

[7] G. A. Moore, "Fabrication Control Plan for the RERTR-12 Experiment," PLN-3254 - Idaho National Laboratory Technical Report., Idaho Falls, 2010.

[8] J. F. Jue, H. P. Blair, R. C. Curtis, A. M. Glenn and D. K. Dennis, "Fabrication of monolithic RERTR fuels by Hot Isostatic Pressing," *J. Nucl. Technol,* vol. 172, no. 2, pp. 204-210, 2010.

[9] D. M. Perez, G. S. Chang, D. M. Wachs and G. A. Roth, "RERTR-12 Irradiation Summary Report, INL/EXT-12-27085," INL, Idaho Falls/ID, 2012.

[10] S. L. Hayes, G. L. Hofman, M. K. Meyer and J. Rest, "Modeling of high density of U-Mo dispersion fuel plate performance," in *24th International Meeting on Reduced Enrichment for Research and Test Reactors (RERTR)*, San Carlos de Bariloche, Argentina, 2002.

[11] Y. S. Kim and G. L. Hofman, "Fission product induced swelling of U–Mo alloy fuel," *Journal of Nuclear Materials,* vol. 419, pp. 291-301, 2011.

[12] Y. S. Kim, G. L. Hofman, J. S. Cheon, A. B. Robinson and D. M. Wachs, "Fission induced swelling and creep of U–Mo alloy fuel," *Journal of Nuclear Materials,* vol. 437, pp. 37-46, 2013.

[13] E. W. Lemmon, M. L. Huber and M. O. McLinden, "NIST Standard Reference Database 23: Reference Fluid

Thermodynamic and Transport Properties - REFPROP, Version 9.0, NIST, Standard Reference Data Program," National Institute of Standards and Technology, Gaithersburg, MD, 2010.

[14] F. P. Incropera and D. P. DeWitt, Introduction to Heat Transfer, Fourth ed., New York, NY: Wiley, ISBN: 0471386499, 2001, pp. 412-417.

[15] R. S. Barnes, "A Theory of swellling and gas release for reactor materials," *J. of Nucl. Mater.,* vol. 11, no. 2, pp. 135-148, 1963.

[16] A. T. Churchman, R. S. Barnes and A. H. Cottrell, "Effects of Heat and Pressure on the Swelling of Irradiated Uranium," *J.Nucl. Energy,* vol. 7, p. 88 96, 1958.

[17] J. B. Rich, G. P. Walters and R. S. Barnes, "The mechanical properties of some highly irradiated Beryllium," *J. of Nucl. Mater.,* vol. 4, no. 3, p. 287–294, 1961.

APPENDIX A

Table A. 1 Material properties for U10Mo

Young's modulus		Density		Yield Stress		Thermal expansion		Thermal conductivity		Specific heat	
[°C]	[GPa]	[°C]	[kg/m^3]	[°C]	[MPa]	[°C]	[10^{-6}/K]	[°C]	[W/m.K]	[°C]	[J/kgK]
21	87.27	25	17130	27	937	25	11.5	25	12.14	0	134.81
200	73.54	100	17060	93	848	100	12.2	100	14.23	100	141.93
400	51.97	200	16970	204	737	200	13.2	200	17.16	200	149.47
600	33.34	300	16880	316	634	300	14.2	300	20.09	300	157.00
		400	16800	427	531	400	15.2	400	23.02	400	164.54
Poisson's Ratio		500	16710	538	428	500	16.2	500	26.37	500	171.66
[°C]	[-]	550	16660	593	373	600	16.6	600	30.14	600	179.19
25	0.324	600	16620			700	17.9	700	33.91	800	193.85
		700	16530			900	20.5	800	37.68	1000	208.92

Table A. 2 Material properties for Zr, Commercially pure, ASTM Grade 702

Young's modulus		Density		Yield Stress		Thermal expansion		Thermal conductivity		Specific heat	
[°C]	[GPa]	[°C]	[kg/m^3]	[°C]	[MPa]	[°C]	[10^{-6}/K]	[°C]	[W/mK]	[°C]	[J/kgK]
21	95.89	25	6499	21	314.70	21.00	5.841	21.00	23.11	21.00	293.3
150	87.36			100	259.90	99.45	6.047	150.25	21.36	128.76	299.25
205	83.68	Poisson's Ratio		149	204.00	148.05	6.178	344.55	20.58	226.37	305.16
292	77.74	[°C]	[-]	197	146.80	196.75	6.279	521.95	21.18	278.05	308.12
370	72.58	25	0.35	259	105.10	300.15	6.532	657.05	22.61	427.33	314.16
426	68.71			297	92.62	349.85	6.653	798.85	24.02	576.61	320.19
516	62.76			348	82.50	401.15	6.754	924.85	25.40	725.89	326.23
611	56.40			400	75.95	450.15	6.876	998.85	26.16	806.28	357.67

Table A. 3 Minimum Creep rate for Grade 702 Zirconium alloy

T = 21 °C		T = 95 °C		T = 205 °C		T = 315 °C		T = 370 °C	
Strain [1/h]	Stress [MPa]	Strain [1/h]	Stress [MPa]	Strain [1/h]	Stress [MPa]	Strain [1/h]	Stress [MPa]	Strain [1/h]	Stress [MPa]
2.878E-08	119.50	2.090E-08	88.22	1.401E-08	54.86	2.949E-08	52.73	3.149E-08	42.13
4.464E-08	134.57	4.521E-08	106.12	2.088E-08	60.97	4.453E-08	57.83	4.510E-08	46.21
1.018E-07	166.20	1.018E-07	129.34	4.457E-08	76.30	1.016E-07	68.66	1.015E-07	55.59
2.173E-07	205.27	2.172E-07	155.59	1.017E-07	94.24	2.196E-07	80.43	2.195E-07	65.13
4.701E-07	253.52	4.697E-07	189.64	2.199E-07	117.93	4.687E-07	94.24	4.684E-07	75.30
1.003E-06	309.01	9.891E-07	228.12	4.693E-07	143.75	1.000E-06	110.40	9.996E-07	88.22
1.641E-06	352.60	2.111E-06	270.81	9.884E-07	177.54	2.106E-06	129.34	2.105E-06	102.00
		3.642E-06	309.01	2.110E-06	219.27	4.495E-06	151.54		
						9.721E-06	175.21		
						2.047E-05	205.27		

Table A. 4 Material properties for Al6061-O

Young's Modulus		Poisson's Ratio		Yield Stress		Thermal Expansion		Conductivity		Specific Heat	
[°C]	[GPa]	[°C]	[-]	[°C]	[MPa]	[°C]	[10^{-6} 1/K]	[°C]	[W/m-K]	[°C]	[J/kg-K]
21	68.26	21	0.330	21	55.16	100	23.6	0	177	17	896
100	65.50	100	0.334	205	55.16	200	24.3	77	186	127	942
150	62.74	150	0.335	230	44.82	300	25.4	177	190	227	988
177	61.36	177	0.336	260	37.92	Density		277	191	327	1034
205	59.29	205	0.336	315	28.96	[°C]	[kg/m^3]	377	188	427	1080
230	57.23	230	0.337	370	20.68	21	2690	477	182	527	1126
260	54.47	260	0.338	425	15.17	93	2690	527	179	582	1151
315	46.88	315	0.360	480	11.03	204	2660				
370	37.92	370	0.400	540	8.27	316	2630				

APPENDIX A

Table A. 5 Thermal creep data for Al6061-O

Time	Strain	STRESS [MPa]				
[h]	[%]	177 [°C]	205 [°C]	260 [°C]	315 [°C]	370 [°C]
0.1	0.1	52.00	41.00	30.00	21.00	14.00
0.1	0.2	55.00	45.00	31.00	22.00	15.00
0.1	0.5	70.00	52.00	34.00	23.00	17.00
0.1	1.0	75.00	55.00	38.00	25.00	17.00
1	0.1	48.00	38.00	27.00	19.00	13.00
1	0.2	52.00	41.00	28.00	20.00	14.00
1	0.5	62.00	45.00	30.00	21.00	15.00
1	1.0	70.00	48.00	32.00	22.00	16.00
10	0.1	41.00	33.00	25.00	16.00	12.00
10	0.2	45.00	34.00	26.00	18.00	12.00
10	0.5	55.00	38.00	28.00	19.00	13.00
10	1.0	62.00	41.00	30.00	20.00	14.00
100	0.1	38.00	30.00	22.00	14.00	10.00
100	0.2	41.00	32.00	23.00	15.00	11.00
100	0.5	52.00	34.00	26.00	17.00	12.00
100	1.0	59.00	38.00	27.00	18.00	12.00
1000	0.1	38.00	28.00	20.00	12.00	9.00
1000	0.2	41.00	30.00	21.00	13.00	10.00
1000	0.5	48.00	31.00	23.00	14.00	10.00
1000	1.0	55.00	32.00	23.00	15.00	11.00

Table A. 6 Yield Stress of AL6061-O with respect to fluence

50 °C		150 °C	
Fluence [n/m^2]	Yield Stress [MPa]	Fluence [n/m^2]	Yield Stress [MPa]
1.00E+25	129.10	1.00E+25	96.03
4.60E+25	162.77	4.60E+25	127.55
1.00E+26	213.34	1.00E+26	174.82
9.60E+26	292.26	1.00E+27	250.18
1.00E+27	295.93		

Table A. 7 Swelling of Al6061

Swelling due to Fluence	
Fluence [n/m^2]	Swelling [%]
1.82E+25	0.01000
2.88E+26	0.16746
1.83E+27	2.02070